Inorganica Chimica Acta 466 (2017) 298–307

Contents lists available at ScienceDirect

Inorganica Chimica Acta

journal homepage: www.elsevier.com/locate/ica

Research paper

Mechanistic study of the substitution reactions of [Pt(II)(bis(2-pyridylmethyl)amine)H_2O]$(ClO_4)_2$ and [Pt(II)(bis(2-pyridylmethyl)sulfide)H_2O]$(ClO_4)_2$ with azole Nucleophiles. Crystal structure of [Pt(II)(bis(2-pyridylmethyl)sulfide)Cl]ClO_4

Slindokuhle V. Nkabinde, Grace Kinunda, Deogratius Jaganyi *

School of Chemistry and Physics, University of KwaZulu-Natal, Scottsville 3209, South Africa

ARTICLE INFO

Article history:
Received 15 November 2016
Received in revised form 3 May 2017
Accepted 22 May 2017
Available online 17 June 2017

Keywords:
Platinum(II)
Substitution
Kinetics
Azoles

ABSTRACT

The substitution kinetics of the complexes [Pt(II)(bis(2-pyridylmethyl)amine)H_2O]$(ClO_4)_2$, **Ptdpa** and [Pt(II)(bis(2-pyridylmethyl)sulfide)H_2O]$(ClO_4)_2$, **Ptdps**, with a series of azole nucleophiles: Imidazole (**Im**), 1-methylimidazole (**MIm**), 1,2-Dimethylimidazole (**DIm**), 1,2,4-triazole (**Trz**) and pyrazole (**Pyz**), were studied in an aqueous medium at constant ionic strength (0.1 M $NaClO_4$). The substitution of the coordinated water ligand on the Pt(II) complexes by the azoles was studied under *pseudo*-first order conditions as a function of the incoming nucleophiles concentration and temperature using either stopped-flow techniques or UV-Vis spectroscopy. **Ptdps** was found to be more reactive (three magnitude higher) than **Ptdpa**. The second-order rate constant, k_2, for all the nucleophiles ranged between 0.087 ± 0.005 and 0.926 ± 0.05 M^{-1} s^{-1} for **Ptdpa** and between 146 ± 4 and 1458 ± 10 M^{-1} s^{-1} for **Ptdps**. The rate of substitution of the aqua ligand is dependent on the strength of the σ-donor character and the π-acceptability of the *trans* atom to the leaving group. The observed reactivity trend for the azoles followed the trend, **MIm** > **Im** > **DIm** > **Trz** > **Pyz**. This reactivity trend correlates with the basicity, steric and electrophilic effects of the nucleophiles. The X-ray crystal structure of **Ptdps–Cl** is reported.

© 2017 Elsevier B.V. All rights reserved.

1. Introduction

Substitution reactions of square planar d^8 complexes, in particular Pt(II) complexes have interested many coordination geneticists. This has been so ever since the serendipitous discovery of the anti-tumor activity of *cis*-[$PtCl_2(NH_3)_2$ (cisplatin). The antitumour activity of this compound and its analogues is due to their covalent binding to or intercalation into certain fragments of nucleic acids [1–4]. However, due to drug resistance and severe side effects associated with the use of cisplatin and analogues, the search has widened to include even non-classical Pt(II) complexes with varied structural properties have been developed. Their kinetic and mechanistic behavior of nucleophillic substitution reactions have also been studied [3–6]. Central to this body of knowledge, has been the kinetic data from mononuclear Pt(II) and Pd(II) complexes with tridentate N^N^N-donor chelate ligands such as diethylenetriamine (dien), [7,8] bis(2-pyridylmethyl)amine (bpma) [9–12] and 2,2′:6′2″-terpyridine (terpy) [13–16]. Their kinetic data have provided useful insight on the reactivity of Pt(II) square planar complexes especially in respect to their modeled interactions with biological target sites such as DNA [10,17,18].

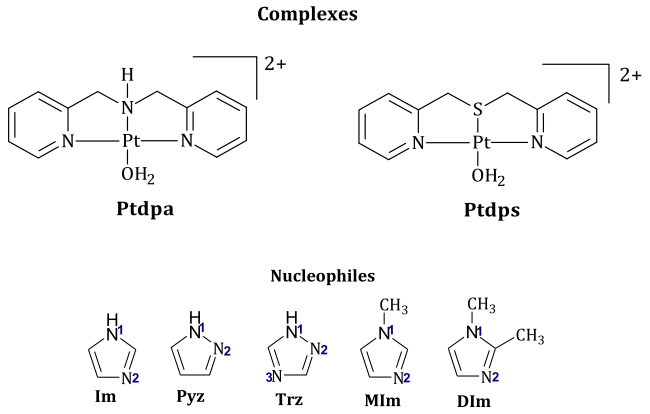
Hofmann and co-workers [16] were able to distinguish between the *trans* and *cis* π/ and σ effect on reactivity for a series of Pt(II) complexes bearing chelating ligands with extended π molecular orbital systems. In their study, the pyridyl nitrogen donor of a terpy ligand backbone was replaced with a phenyl carbon donor on the *trans* and *cis*-positions in order to investigate the influence of having a strong σ-donor group on either *cis* or *trans* to the leaving group on the substitution reactions of the Pt(II) complexes. The Pt(II) complex with the phenyl carbon donor in the *cis*-position resulted in a decrease in the substitution rate due to the accumulation of electron density at the metal centre [16,19]. Unlike this complex, its isomeric analogue with the phenyl ring on the *trans* position showed a significant increase in reactivity compared to the Pt(II) terpy complex. This was due to the high destabilization of the ground state *via* the *trans* influence and its own additional π-acceptor contribution on the chelate [16].

* Corresponding author.
E-mail address: jaganyi@ukzn.ac.za (D. Jaganyi).

http://dx.doi.org/10.1016/j.ica.2017.05.054
0020-1693/© 2017 Elsevier B.V. All rights reserved.

Work conducted by Mambanda et al. [18] showed that attaching alkyl hydrocarbon groups of varying chain lengths on the *trans*-N donor atoms of Pt(Cl) bis(2-pyridylmethyl)amine complex enhances the substitution reactivity of the parent complex. This was due to the additional σ-inductive donation brought about by the alkyl chain. The increase in reactivity was dependent on the chain length and branching of the alkyl groups [18]. Furthermore, work reported by Hochreuther et al. [20] on the diaqua complex, [Pt(2-methylthiomethylpyridine)$(OH_2)_2$]$^{2+}$, Pt(mtp) confirmed that the first substitution occurs at the aqua ligand *trans* to the strong σ-donor sulfur atom. This was ahead of the one coordinated to the strong π-acceptor pyridine ring of the 2-methylpyridine ligand [20,21]. However, a study conducted by Pitteri et al. [14] on the substitution reactions of Pt(II) complexes with bis(2-pyridylmethyl) sulfide and terpy using halide nucleophiles showed comparable reactivities between them. The results meant that the *trans*-labilizing effect of a coplanar pyridine ring of terpy was almost the same as that of the thioether sulfur atom [14]. In another study by this group, the results obtained showed the rate of substituting the pyridine from [Pt(bis(2-pyridylmethyl)sulfide) pyridine] was greater than from [Pt(bis(methylthiomethyl)pyridine]. This was even greater than from [Pt(bis(2-pyridylmethyl) amine)pyridine] [22]. The *trans* effect of the sulfur atom of the thioether and to a lesser extent, the π-acceptability of this *cis* pyridine rings controlled the reactivity of the Pt(II) complex.

This work reports on the substitution reactions of [Pt(bis(2-pyridylmethyl)amine)(H_2O)]$(ClO_4)_2$ (**Ptdpa**) and [Pt(bis(2-pyridylmethyl)sulfide)H_2O]$(ClO_4)_2$ (**Ptdps**) with neutral nitrogen donor azole nucleophiles. The nucleophiles used are imidazole (**Im**), 1-methylimidazole (**MIm**), 1,2-dimethylimidazole (**DIm**), pyrazole (**Pyz**) and 1,2,4-triazole (**Trz**). The five-membered neutral heterocyclic nucleophiles containing either 2 or 3 N-atoms (azoles) are important model donors from a bioinorganic point of view. Studies have shown that Pt(II) complexes prefer binding to DNA through the N7 atom of guanine (part of its ring structure is an azole) instead of adenine, leading to a distorted DNA strand [23–27]. Furthermore, the imidazole groups of histidine residues form part of the coordinated ligands in most metalloproteins [23,28–31]. The structures of the investigated complexes and nucleophiles are illustrated in Scheme 1.



Scheme 1. Structures of the Pt(II) complexes and nucleophiles used in the study.

2. Experimental

2.1. Chemicals and reagents

Thiosemicarbazide (99%), 2-picolyl chloride hydrochloride (98%), di-(2-picolyl) amine (**dpa**) (99%), sodium perchlorate ($NaClO_4$), silver perchlorate ($AgClO_4$), pyrazole (98%), 1,2,4-triazole (98%), 1-methylimidazole and 1,2-dimethylimidazole were purchased from Aldrich and were used as received. The Pt(II) precursor complexes, dichlorobis(benzonitrile)Pt(II), ([Pt$(Ph(CN)_2Cl_2]$ (99%) and potassium tetrachloroplatinate, K_2PtCl_4 (99.99%) were purchased from Strem Chemicals and were used as supplied. All organic solvents along with the acids, ($HClO_4$, HCl) were supplied by Merck except for nitromethane which was purchased from Saarchem.

2.2. Synthesis of (bis(2-pyridylmethyl)sulfide), dps

The ligand, **dps**, was synthesized following a literature method [32]. Thiosemicarbazide (0.46 g, 6.1 mmol) was dissolved in 150 mL distilled H_2O. To the solution, was added 2-picolyl chloride hydrochloride (3.30 g, 20.1 mmol) followed by NaOH (8.09 g, 202 mmol). The resulting mixture was stirred at room temperature for 24 h and the unreacted material was removed by filtration. The filtrate was extracted using 3 portions of 50 mL $CHCl_3$ and the combined organic extracts were dried over anhydrous $MgSO_4$. After filtering off the $MgSO_4$, the solvent was removed completely under *vacuo*. The desired ligand (**dps**) was obtained as brown oil.

Yield: 1.15 g (87%). TOF MS ES$^+$: m/z = 239.06 [M + Na]. ^{1}H NMR ($CDCl_3$, 400 MHz): δ/ppm = 8.51 (1H, d), 7.60(1H, td), 7.34 (d, 1H). 7.12(ddd, 1H), 3.80(s, 2H), 2.59(s, 2H).

2.3. Synthesis of Pt(II) complexes

2.3.1. Synthesis of [Pt(bis(2-pyridylmethyl)amine)Cl](ClO4), ptdpa–cl

The complex, **Ptdpa–Cl** was synthesized according to a well-known procedure [33]. To a solution of K_2PtCl_4 (0.205 g, 0.48 mmol) dissolved in 0.005 M HCl (100 mL), the ligand **dpa** (0.087 mL, 0.48 mmol) was added. The mixture was refluxed for 3 days and during this period; a yellow suspension formed which redissolved later. The yellow mixture was cooled to room temperature then filtered and the filtrate was reduced to about 10 mL. Addition of saturated $NaClO_4$ (3 mL) precipitated the desired complex as a yellow colloid. This was collected by filtration, washed with small amounts of water, ethanol and ether and was dried under vacuum.

Yield: 242 mg (95%). Anal. Calcd for $C_{12}H_{13}N_3O_4PtCl_2$: C = 27. 23; H = 2.48; N = 7.94. Found: C = 26. 73; H = 2.45; N = 7.62. TOF MS ES$^+$: m/z = 430.0519 (M^++Na). ^{1}H NMR (DMSO-d_6, 400 MHz) δ/ppm: 8.75 (d, 2H); 8.57 (br s, 1H); 8.18 (t, 2H); 7.71 (d, 2H); 7.57 (t, 2H); 4.88 (m, 2H); 4.55(dd, 2H). ^{13}C NMR (DMSO-d_6, 400 MHz) δ/ppm: 167.5; 147.5; 139.5; 124.0; 121.3; 57.6. ^{195}Pt NMR (DMSO-d_6, 500 MHz) δ/ppm: −2346.2. IR (4000-650)[†] $\bar{\nu}$: 3096(mb), 2920(w), 1615(sb), 1483(w), 1436(mb), 1219(m), 1082 (vs), 1021(m), 765(vs).

2.3.2. Synthesis of [Pt(bis(2-pyridylmethyl)sulfide)Cl](ClO4), ptdps–cl

The complex, **Ptdps–Cl** was obtained following a literature method [34]. To [Pt$(Ph(CN)_2Cl_2]$ (1.50 g, 3.0 mmol) dissolved in a minimum amount of CH_2Cl_2 was added a solution of the ligand (0.649 g, 3 mmol in 10 mL CH_2Cl_2) drop wise. The mixture was refluxed for 2 h, and during this time a yellow precipitate gradually appeared. The crude product was filtered off under *vacuo* as a yellow solid. The product was recrystallized from a supersaturated and boiling aqueous solution of $LiClO_4$ which was slowly cooled to room temperature and the desired compound filtered off using a 0.45 μm nylon filter membrane.

Yield: 1.05 g (64%). Anal. Calcd for $C_{12}H_{12}N_2SO_4PtCl_2$: C = 26.38; H = 2.21; N = 5.13. Found: C = 25.91; H = 2.06; N = 5.47. TOF MS ES +: m/z = 239 [M + Na]. ^{1}H NMR (DMSO-d_6, 400 MHz) δ/ppm: 8.92

[†] vs = very strong, s = strong, m = medium, w = weak and b = broad.

(d, 2H); 8.20(t, 2H); 7.84(d, 2H); 7.61(t, 2H); 5.75(d, 2H); 4.81(d, 2H). ^{13}C NMR (DMSO-d_6, 400 MHz) δ/ppm: 165.3; 150.6; 140.9; 125.4; 124.9; 44.2. ^{195}Pt NMR (DMSO-d_6, 500 MHz) δ/ppm: -2694.02. IR ***(4000-650)† $\bar{\nu}$: 3297(w), 3167(wb), 2918(m), 1622(sb), 1476(w), 1445(w), 1358(w).

2.3.3. Crystallization of [Pt(bis(2-pyridylmethyl) sulfide)Cl](ClO$_4$)·CH$_3$NO$_2$, ptdps–cl

The crystal, **Ptdps–Cl** was obtained by dissolving [Pt(bis(2-pyridylmethyl) sulfide)Cl](ClO$_4$) in 3 mL nitromethane to make a saturated solution and undissolved materials were filtered through a 0.45 μm nylon filter membrane. The brown crystal was grown through slow vapour diffusion of ether into the solution contained in a special designed chamber. The crystal structure is shown in Fig. 2 and details of the crystal data and structure refinement are shown in Table 1.

2.4. Preparation of aqua complex solutions for kinetic analysis

The solution of the aqua complexes, **Ptdpa** and **Ptdps** were prepared as described in the literature [33] by reacting an appropriate amount of AgClO$_4$ with the corresponding chloro complexes. The chloro Pt(II) complex and AgClO$_4$ (1:1 M ratio) were dissolved in 0.10 HClO$_4$ solution and the mixture was stirred under a flow of nitrogen at 40–50 °C in the dark for 24 h. The silver chloride precipitate which formed was filtered off using a 0.45 μm nylon filter membrane. The filtrate was collected and the pH was maintained at 1 by diluting with 0.10 M HClO$_4$ solution to give solution with the final concentration of 2×10^{-5} M for both complexes.

2.5. Physical measurements and instrumentation

The NMR spectra were recorded on a Bruker Avance III 500 or Bruker Avance III 400 at frequencies of 500 MHz or 400 MHz (^{1}H) and 125 MHz/100 MHz (Pt) using either a 5 mm BBOZ probe or a 5 mm TBIZ probe. All proton and carbon chemical shifts are reported relative to the relevant solvent signals at 30 °C unless stated otherwise. Elemental compositions of the ligands and complexes were performed on a Thermo Scientific Flash 2000. The pH of the aqueous solutions of the complex, **Ptdps**, was measured using a Jenway 4330 Conductivity/pH meter equipped with a Micro 4.5 μm diameter glass electrode. The electrode was calibrated at 25 °C using standard buffer solutions of pH 4.0; 7.0 and 10.0 (Merck). The electrolyte of pH electrode was replaced with 3.0 M NaCl instead of KCl to prevent precipitation of KClO$_4$ during pH measurement. The mass spectral data of the ligands and complexes were acquired on a Waters Micromass LCT Premier spectrometer. All FTIR spectra were recorded on a Bruker Alpha FTIR spectrometer. The spectra were acquired by crushing the powder on the sample platform between the Diamond Heads. A total of about 25 spectra were averaged. Relevant information acquired and within the frequency range 4000–650 cm^{-1}. An Applied Photophysics SX 20 stopped-flow spectrophotometer coupled to an online data acquisition system was used to monitor fast reactions. Slow reactions were monitored using a Varian UV/Vis Cary 100 spectrophotometer. The temperature of these instruments was controlled throughout all kinetic measurements to ±0.02 °C. pK_a and kinetic traces were graphically analysed using the Origin 7.5® [35] software package.

2.6. Determination of the pK$_a$ value of Ptdps

Spectrophotometric pH titrations of the aqua complex, **Ptdps** with the base, NaOH were performed in the pH range of 1–10 and monitored using an UV-Vis spectrophotometer. To avoid dilution effects, a large complex solution volume of 150 mL was used and crushed NaOH pellets were added to increase the pH stepwise from pH 1 until pH 3. Further increases in pH were achieved by drop wise additions of a series of NaOH solutions of the concentrations ranging from 0.01 M to 0.5 M. 2.0 mL aliquots from the complex solution were withdrawn for pH measurement; these were discarded to avoid *in situ* contamination by chloride ions released from the pH electrode. The UV-Vis spectra for the pH titration along with an inset of the plot of the absorbance versus pH at 300 nm fitted using the Boltzmann equation are shown in Fig. 1 and the pK_a value is given as footnote in Table 4. It is worth noting that the pKa value of **Ptdpa** was extracted from literature [33].

2.7. X ray crystallography

The single crystal X-ray data for the metal complex was recorded on a Bruker Apex II Duo equipped with an Oxford Instrument Cryojet operating at 100 K and an Incoatec microsource operating at 30 W power. The data was collected with Mo Kα (λ = 0.71073 Å) radiation at a crystal-to-detector distance of 50 mm. The following conditions were used for the Bruker data collection: omega and phi scans with exposures taken at 30 W X-ray power and 0.50° frame widths using APEX2 [36]. The data was reduced with the program SAINT [36] using outlier rejection, scan speed scaling, as well as standard Lorentz and polarisation correction factors. Direct methods, SHELXS-97 [37] were used to solve the structure. Hydrogen atoms were located in the difference density map and refined isotropically with SHELXL-97 [37] and were included as idealised contributors in the least squares process. OLEX2, a complete structure solution, refinement and analysis program [38] was used to prepare the material for publication. The crystal structure is shown in Fig. 2.

3. Computational details

The density functional (DFT) calculations of the complexes, **Ptdpa**; **Ptdps** and **Ptdps–Cl** modelled as cations and in the gas phase were performed with the Gaussian 09W computational software [39] using the B3LYP functional in the basis set of LANL2DZ for the electronic structures at the ground state. A summary of the computational data is illustrated in Table 2 while the HOMO-LUMO diagrams depicted in Fig. 3.

3.1. Kinetic measurements

All kinetic reactions were carried out under *pseudo*-first order rate conditions. A pH of 2.0 and an ionic strength of 0.1 M NaClO$_4$ were maintained throughout the kinetic experiments. Suitable wavelengths at which kinetic measurements were collected were predetermined spectrophotometrically by monitoring the change in absorbance of the mixture of the Pt(II) complex and the nucleophile as a function of time and these are summarised in the supporting information. The temperature dependence studies for all the reactions were studied within temperatures ranging from 15 to 40 °C at an interval of 5 °C.

4. Results

4.1. Crystal structure of [Ptdps–Cl](ClO$_4$)·CH$_3$NO$_2$

The complex, **Ptdps–Cl(ClO$_4$).CH$_3$NO$_2$** crystallized in the monoclinic space group, $P2_1/c$ and contained one complete molecule with Z = 4 as shown Fig. 2. Crystal data is summarised in Tables 1 and 2.

The complex crystallises with a perchlorate (ClO$_4$) counter ion and nitromethane (CH$_3$NO$_2$) solvent molecule. The tridentate ligand,

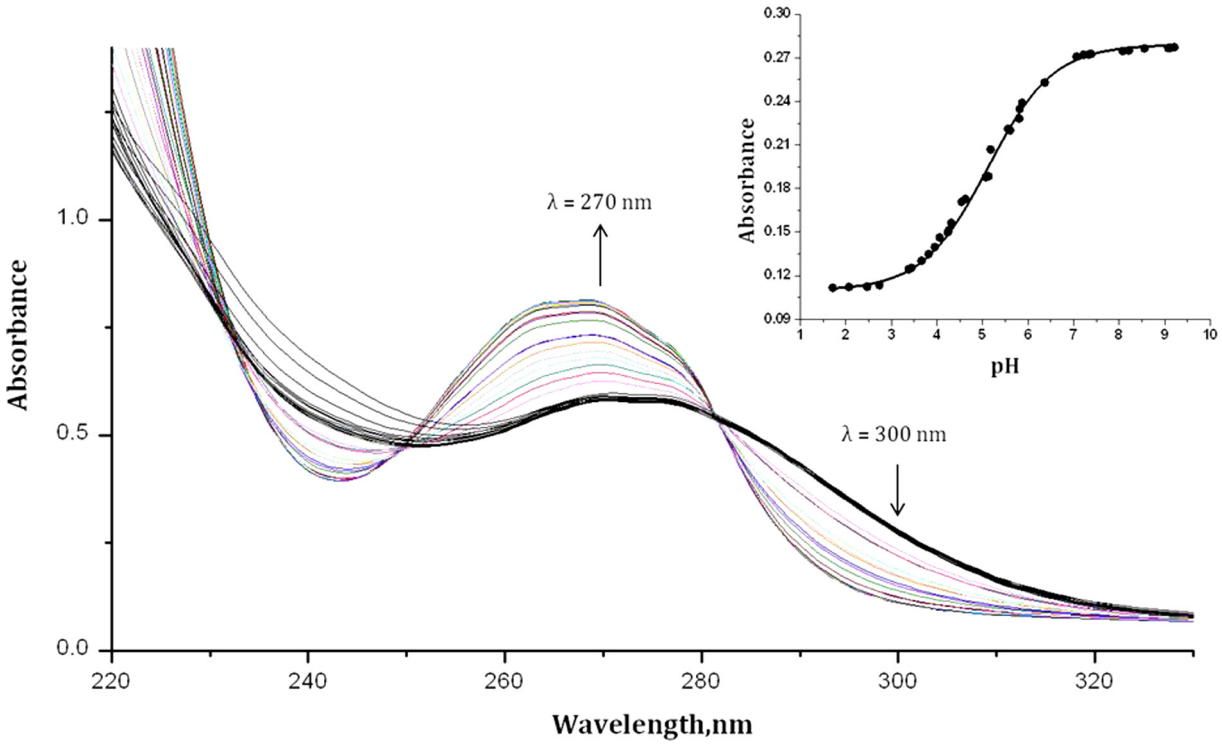


Fig. 1. UV–Vis spectra for the titration of 0.1 mM **Ptdps** with NaOH at pH range 1–10, T = 298 K. *Inset*: Plot of absorbance vs pH at 300 nm.

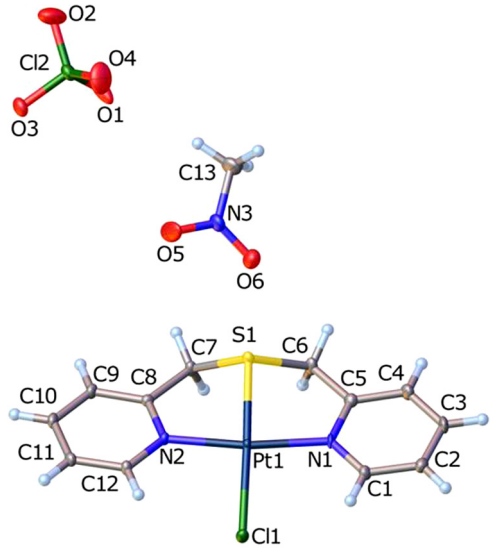


Fig. 2. Thermal ellipsoid diagram (50% probability surfaces) of the molecular structure of **Ptdps–Cl (ClO_4) CH_3NO_2.**

Table 1
Crystallographic data and structure refinement for [**Ptdps–Cl**](**ClO_4**)·**CH_3NO_2**].

Parameter	
Chemical formula	$C_{12}H_{12}ClN_2PtS{\cdot}ClO_4{\cdot}CH_3NO_2$
M_r (g mol^{-1})	607.33
Crystal system	Monoclinic
Space group	$P21/c$
Temperature (K)	100
a (Å)	14.6795 (5)
b (Å)	7.2800 (3)
c (Å)	17.2174 (6)
β (°)	103.086 (2)
V (Å^3)	1792.19 (11)
Z	4
Radiation type	Mo Kα
Crystal size (mm)	0.28 × 0.20 × 0.10
T_{min}/T_{max}	0.205, 0.491
No. of measured, independent and observed [I > 2σ(I)] reflections	18487, 5463, 5101
R_{int}	0.026
(sin Θ/λ)$_{max}$ (Å^{-1})	0.715
$R[F^2 > 2\sigma(F^2)]$, $wR(F^2)$, S	0.026, 0.066, 1.05
No. of parameters	236
No. of restraints	0
H-atom treatment	H-atom parameters constrained
Δ›$_{max}$, Δ›$_{min}$ (e Å^{-3})	3.41, −3.07

dps, coordinates to the Pt(II) centre by the nitrogen atoms on the *cis*-positioned pyridine rings and the S-donor of the *trans*-situated thioether group while the fourth position is occupied by a chloride ion, see Fig. 2. The coordination geometry of the complexes is a slightly distorted square planar. Its N2–Pt1–N1 bite angle is deviated from linearity to an angle of 168.2(10)°. The N2–Pt–S1 angle is 84.7 (7)° while the N1–Pt1–S1 angle is similar to it at 85.3(7)°. The S1–Pt–Cl angle is slightly lower than 180° at 178.3(2)°.

Due to the bigger size of the S-atom, the thioether group is forced out of the plane containing the rest of the molecule as a way of minimizing non-bonding/bonding electron-electron repulsions. This can be seen clearly from Fig. S2 (Supporting information). As a result, the methylene groups of the chelate are located on one side and the chloro leaving group tipped over on the other side exposing it to nucleophillic attacks.

From Table 2 it is noticeable that the Pt–Cl bond (2.323(6) Å) is significantly longer than the Pt1–S1 bond (2.228(6) Å). In the solid and also in solution, the elongation of the Pt–Cl bond is due to the strong *trans* influence of the *trans* bonded sulfur atom. This is in line with the big size of the sulfur atom and high diffusity of its atomic orbitals which leads to a strong bond formation with the soft Pt(II) atom. This weakens the Pt–Cl bond *trans* to the thioether. In addition, it tips off the leaving group from the molecule plane making it prone to aerial attack on one side.

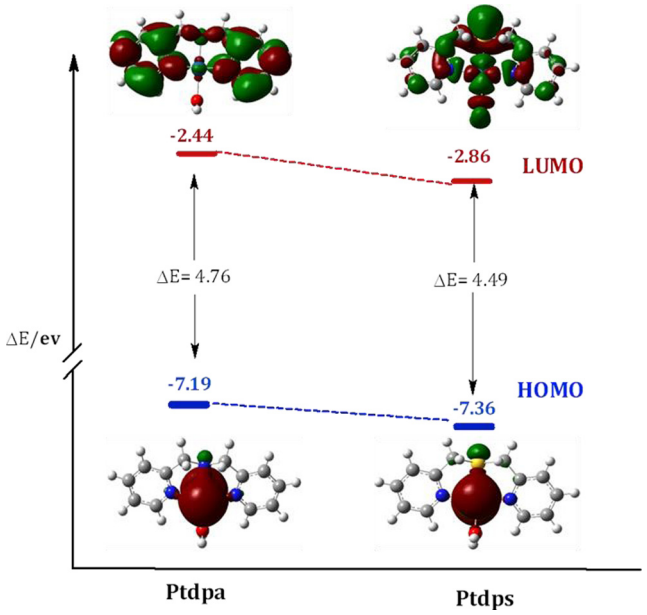


Fig. 3. Density functional theoretical (DFT) minimum energy structures, HOMO and frontier molecular orbitals for the complexes **Ptdpa** and **Ptdps**.

Table 2
Selected X-ray determined bond lengths (Å) and angles (°) for **Ptdps–Cl.**

Bond lengths (Å)			
Pt1–N2	2.015 (2)	C7–C8	1.503 [4]
Pt1–N1	2.027 (2)	C7–H7A	0.9900
Pt1–S1	2.2277 (6)	C7–H7B	0.9900
Pt1–Cl1	2.3228 (6)	C8–C9	1.389 [3]
Angles (°)			
N2–Pt1–N1	168.24 (10)	C8–C7–S1	106.79 [18]
N2–Pt1–S1	84.70 (7)	C8–C7–H7A	110.4
N1–Pt1–S1	85.33 (7)	S1–C7–H7A	110.4
S1–Pt1–Cl1	178.31 (2)	H7A–C7–H7B	108.6

4.2. Computational studies

Computational calculations were performed at the DFT level of theory and the data is summarised in Table 3 and Fig. 3. The planarity and ESP diagrams for both complexes are included in the Supporting information, Table S2.

To compare the accuracy of the calculated data in the gaseous state, X-ray data of **Ptdps–Cl(ClO4).CH_3NO_2** was compared with the computed data for **Ptdps–Cl** in the gaseous state. The calculated bond lengths and angles showed a good match with those obtained for the crystal structure within the experimental error. The mapping of HOMOs of **Ptdpa** and **Ptdps** (Fig. 3) are similar. The HOMO orbitals are situated mainly on the metal centre. However, the LUMOs are distinctive in their mapping and relative energies. For **Ptdps**, the LUMO is markedly mapped along the S_{trans}–Pt–O bonds axes and extended towards the methylene groups and pyridine groups. It is also energetically more stable than that of **Ptdpa**. Some notable differences on the electron isodensity of LUMO of **Ptdpa** are that its mapping on the N donor atom is relatively lower compared to that on the S donor atom of the **Ptdps** and is also more pronounced on the pyridyl rings of the ligand than on the N atom. A more stable LUMO (which is of anti-bonding character) on **Ptdps** which is more pronounced on the S donor atom means the coordinated **dps** ligand is a better π∗-acceptor of electron density from the metal *d*-orbitals compared to **dpa**. This is so because the S-atom of **dps** can readily uses its low-lying energy atomic orbitals (4d) to form extended π-molecular orbitals with the methylene carbon and the lateral pyridyl ring atoms within the entire ligand. Thus, the amine N donor atom of **dpa** is relatively isolated from the pyridyl acceptor rings and less effective in accepting electron density via back bonding. Through back bonding ($5\pi*_{\text{ligand centred}} \leftarrow d_{(\text{metal centred})}$) [40], the Pt ion of **Ptdps** is expected to be more electrophilic as observed by a more positive electrophilicity index in the DFT calculations [41]. According to the HASB theory, the higher polarisability of S will also result in a stronger σ-bonding to the soft Pt atom [22]. As a consequence, the combined influence of the stronger σ-donation

Table 3
A summary of the DFT calculated structural data for the investigated tridentate Pt(II) complexes, **Ptdpa** and **Ptdps** at B3LYP/LANL2DZ level of theory.

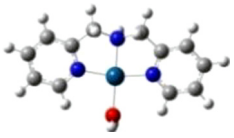
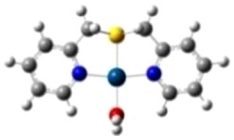
Properties	Ptdpa	Ptdps	Ptdps–Cl	X-ray Data
				
BOND LENGTHS (Å)				
Pt – N/S_{trans}	2.022	2.356	2.396	2.2277 [6]
Pt – O/Cl	2.105	2.122	2.442	2.3228 [6]
BOND ANGLES (°)				
O – Pt – N_{cis}	96.67	93.04	94.61	93.62 [7]
O – Pt – N/S_{trans}	180.0	177.22	175.2	178.31 [2]
N_{cis} – Pt – N_{cis}	166.4	167.8	168.6	168.24 [10]
ENERGY GAP, ΔE (eV)				
HOMO	−7.19	−7.36		
LUMO	−2.44	−2.86		
ΔE/eV	4.75	4.49		
CHEMICAL HARDNESS, η (eV)	2.38	2.25		
ELECTROPHILICITY INDEX, ω (eV)	4.88	5.80		
NBO CHARGES				
Pt^{2+}	0.775	0.604		
O^{2-}	−0.924	−0.921		
N/S_{trans}	−0.629	0.443		
N_{cis}	−0.517	−0.513		
DIPOLE MOMENT (Debye)	0.270	3.663		

Table 4
Summary of k_2 values and activation parameters, $\Delta H^{\neq}$ and $\Delta S^{\neq}$ for **Ptdpa** and **Ptdps** with azole nucleophiles.

Nu	k_2 (M^{-1} s^{-1})	$\Delta H^{\neq}$ (kJ mol^{-1})	$\Delta S^{\neq}$ (J K^{-1} mol^{-1})
Ptdpa			
Im	0.451 ± 0.01	49 ± 3	−87 ± 10
MIm	0.926 ± 0.05	53 ± 10	−202 ± 2
DIm	0.311 ± 0.007	63 ± 3	−43 ± 11
Trz	0.267 ± 0.008	57 ± 4	−70 ± 10
Pyz	0.087 ± 0.005	71 ± 4	−30 ± 10
Ptdps			
Im	950 ± 10	54 ± 3	−58 ± 9
MIm	1460 ± 10	52 ± 2	−65 ± 6
DIm	720 ± 10	56 ± 2	−59 ± 7
Trz	263 ± 5	63 ± 5	−40 ± 20
Pyz	146 ± 4	12.0 ± 0.7	−155 ± 2

Thermodynamic data: pK_a values: **Ptdpa** = 5.53 ± 0.07[1] **Ptdps** = 5.12 ± 0.04[2].
[1] Value extracted from literature, Ref. [33].
[2] Value from current study determined by fitting the data to the Boltzmann equation, $y = A_2 + (A_1 - A_2)/(1 + \exp((x - x_0)/dx)$, using the Origin 7.5® program.

toward the metal centre and strong π-acceptability of the **dps** ligand labile the coligand of **Ptdps** to a greater extent than **dpa**, resulting in a higher rate of substitution in **Ptdps**.

4.3. Kinetic studies

The substitution of the coordinated aqua ligands from Pt(II) tridentate complexes, **Ptdpa** and **Ptdps** by five azole nucleophiles, **Im**, **MIm**, **DIm**, **Trz** and **Pyz** were investigated as a function of concentration and temperature. Both conventional UV-Vis and stopped-flow techniques were used to monitor the reactions under *pseudo* first-order conditions. Substitution reactions of **Ptdpa** with all nucleophiles were studied using a UV-Vis spectrophotometer within the range of 200–800 nm. Fig. 4 shows typical changes in the absorption spectra of **Ptdpa**. The kinetic trace at 275 nm is shown as an inset to the figure. Substitution reactions of **Ptdps** were all followed using stopped-flow spectrophotometry and all kinetic traces obtained were described by single exponential fits. A typical stopped-flow trace for **Ptdps** with methyl imidazole, **MIm** at 298 K is presented in Fig. 5.The *pseudo* first-order rate constants, k_{obs}, were calculated from the kinetic traces. Fig. 6 illustrates the plot of the dependence of the *pseudo* first-order rate constant (k_{obs}) on the entering nucleophile concentration for **Ptdps** from which the second-order rate constants, k_2 are obtained from the slopes of the linear plots and the data is summarised in Table 4. Since all plots had zero intercepts, the reactions were considered irreversible and independent of the solvent effect. The overall rate law for the mechanism of the aqua substitution by the azole is according to Eq. (1).

$$k_{obs} = k_2[Nu] \quad (1)$$

Kinetic measurements were also carried out at different temperatures to obtain k_2 values for calculating entropy of activation ($\Delta S^{\neq}$) and enthalpy of activation ($\Delta H^{\neq}$). These were obtained from the Eyring plots [24,25] (Fig. 7). The activation data from the plots are summarised in Table 4.

5. Discussion

In this study, two Pt(II) complexes, **Ptdpa** and **Ptdps** were synthesized and their substitution reactivity with a set of azole nucleophiles was investigated in order to understand the effect of changing the *trans*-donor from an amine to a thioether group. Data from Table 4 shows the aqua substitution by N-donor nucleophiles is about three orders of magnitudes greater for **Ptdps** than it is for **Ptdpa**. For instance, the reaction between **Ptdps** and **MIm** is 1.6×10^3 times faster than **Ptdpa**. A similar comparison shows that a reaction between **Ptdps** and **Trz** is in fact 2.6×10^3 times faster than **Ptdpa**. Therefore it is clear that the reactivity trend among the two Pt(II) complexes is electronically controlled. The substitution reactivity trend for all the nucleophiles investigated follows the order **MIm** > **Im** > **DIm** > **Trz** > **Pyz** for both complexes, reflecting that the nucleophilicity trend was both sterically and electronically controlled.

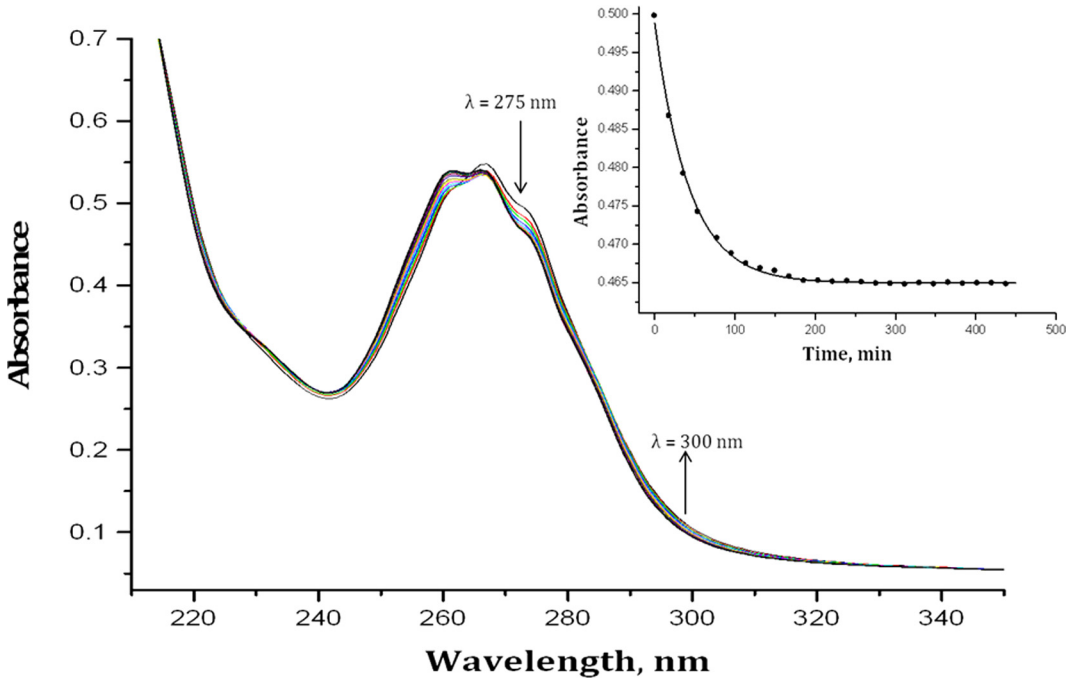


Fig. 4. UV-Vis absorbance spectra for **Ptdpa** (1.032×10^{-4} M) and **Trz** (1.03×10^{-3} M), I = 0.1 M $NaClO_4$, T = 298 K. *Inset*: Kinetic trace at 275 nm.

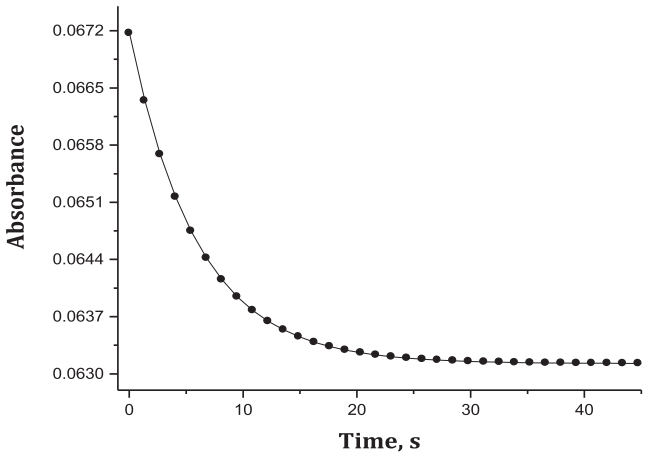


Fig. 5. Stopped-flow kinetic trace at 285 nm for the substitution reaction of **Ptdps** with **Pyz** at 298 K.

The high reactivity of **Ptdps** towards the N-donor nucleophiles is attributed to the strong σ-donor S-atom *trans* to the leaving group. This significantly labializes the *trans* water ligand due to the increased *trans* effect [20]. This is in agreement with the work reported by Pitteri et al. when a series of neutral and anionic nucleophiles were used [22]. As explained, the strong σ-*trans* effect of the thioether elongates the Pt–O bond of the aqua (2.122 Å) as compared to the Pt–O bond in **Ptdpa** (2.105 Å). This is reflected in the DFT-calculated bond lengths at the ground state shown in Table 2. This is in excellent agreement with previous studies showing that when the σ-donor ability of the *trans* ligand is enhanced so does the *trans* labialization effect of the metal-to-leaving group bond [22,42,43]. Another factor to consider is that sulfur is a much larger atom than nitrogen; therefore it is easily polarizable due to high diffusity of its atomic orbitals compared to that of nitrogen which further explains the higher reactivity of **Ptdps** to that of **Ptdpa** [22,42,43]. Due to the presence of pyridyl moieties in the *cis*-position of both the complexes, their π-back bonding ability is similar. This is supported by the DFT calculated NBO charges on the N_{cis} atoms shown on Table 2, (−0.517) for **Ptdpa** and (−0.513) for **Ptdps.** The Pt(II) ion of **Ptdpa** with NBO charge 0.775 is more electropositive than that of **Ptdps** (0.604). This decrease in positivity of the metal centre from **Ptdpa** to **Ptdps** can be accounted for by the strong σ-donor character of the *trans*-thioether moiety in **Ptdps**. Electrons are donated from the strong S- or N-donor *via* the σ-bond to the metal centre in **Ptdps** or **Ptdpa**, respectively. The results show that the *trans*-effect is much stronger than the repulsion effect of the incoming nucleophile due to a higher electron density on the Pt-atom.

Apart from the σ-donor ability of the *trans*-S atom of the thioether group, the high reactivity of **Ptdps** compared to **Ptdpa** is also due to the better ability of thioether in **dps** to receive electron density. The S-atom of **Ptdps** is able to accept electron density from the metal centre through π-back bonding using the low lying vacant *d*-orbitals of the sulfur atom. In this case, the S-atom of the thioether group of **Ptdps** acts as both σ-donor and π-acceptor. This is supported by the DFT relative energies of the LUMO (Fig. 3) and the pK_a values (Table 4) which is an indication of the electronic distribution around the metal centre [20,44].

The level of reactivity of **Ptdps** can be compared to that of Pt (II) complexes **Pt(L)Cl** (L = 1,3-di(2-pyridyl)benzene) [45] using similar azoles, even though the leaving group differs. The common driving force between the two complexes is *trans* influence of on rate of substitution. In case of **Pt(L)Cl**, the large kinetic *trans*-effect of the σ-bound carbon and the increase in the π-back bonding due to the in-plane aryl ligand are responsible for the observed substitution which is similar to the properties of the S-atom in the **Ptdps** complex.

It is known that the substitution reactions of square planar Pt(II) complexes depend highly on the nature of the entering nucleophile [46–48]. As such, the nucleophilicity of the nucleophiles selected for this study depends on both their electronic and steric properties. To explain the reactivity trend of the nucleophiles, the investigated azole nucleophiles were separated into two groups based on their structural similarities. The first group comprises of imidazoles which differed only in the number of methyl substituents on

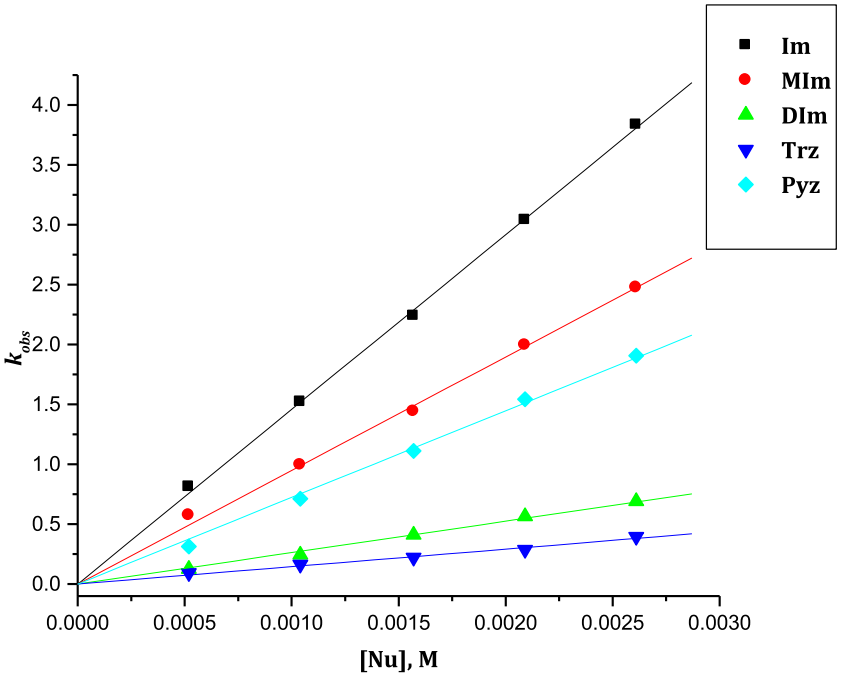


Fig. 6. Concentration dependence plot for the displacement of the aqua ligand from **Ptdps** (2×10^{-5} M) by azole nucleophiles at 298 K.

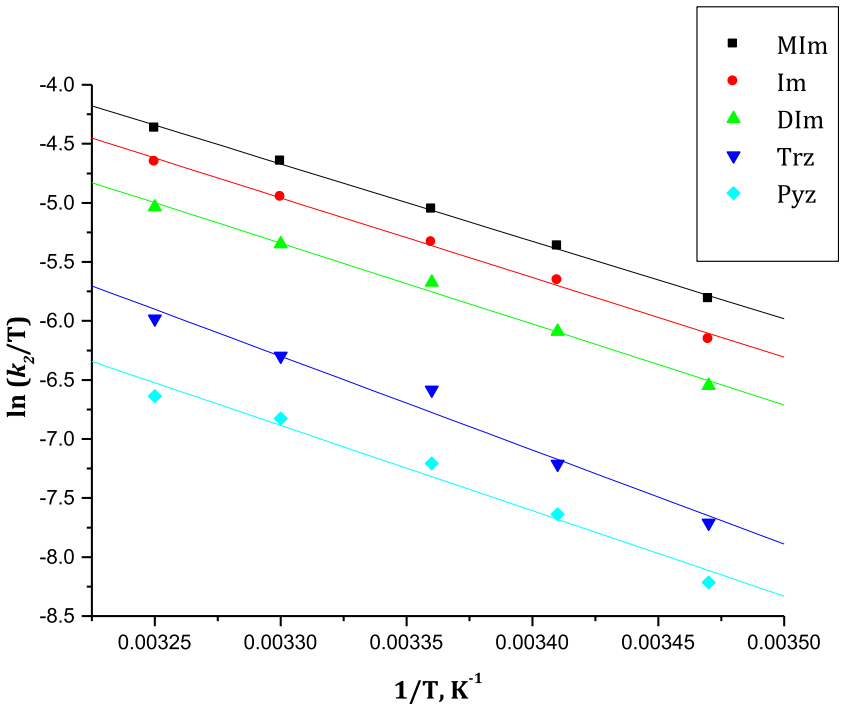
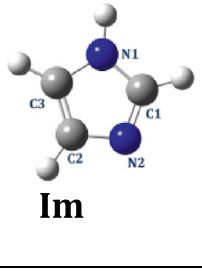
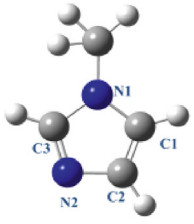
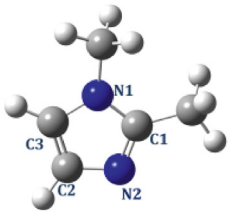
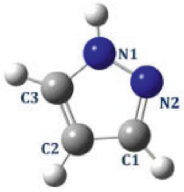
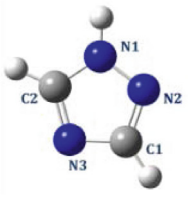


Fig. 7. Temperature dependence of k_2/ M^{-1} s^{-1}, for the displacement of the aqua ligand in **Ptdps** (2×10^{-5} M) by a series of azole nucleophiles.

Table 5
The pK_a values and NBO charges for the donor atoms of the nucleophiles studied.

	Im	MIm	DIm	Pyz	Trz
					
N1	−0.552	−0.415	−0.416	−0.351	−0.431
N2	−0.480	−0.494	−0.496	−0.294	−0.272
N3	–	–	–	–	−0.490
pK_a*	7.00	7.33	8.00	2.52	2.19

* pK_a values from Ref. [50].

the ring, *viz.*, imidazole (**Im**), 1-methyl imidazole (**MIm**) and 1,2-dimethyl imidazole (**DIm**). The other group consists of azoles with no substituents, **Im**, **Pyz** and **Trz**. Of the imidazoles used, **DIm** represents the most sterically hindered nucleophile in the series due to the steric effect of its 2-methyl substituent. As a result, **DIm** showed the slowest reactivity with both Pt(II) complexes when compared to **MIm** and **Im**, which have one and no substituents on their rings respectively. In contrast, **MIm** is more reactive than **Im** despite the steric hindrance due to the substituent on the former. The higher reactivity of **MIm** as compared to **Im** is attributed to the σ-effect due to the methyl substituent presented in the N1 atom [27,49]. The methyl group inductively donates electrons to the ring system, causing the N2- donor to be more basic. Due to the methyl group being situated far from the expected N2 binding position, steric hindrance is minimal [45,49]. Thus, the overall order in reactivity for the imidazoles follows the trend **MIm** > **Im** > **DIm**. However, other studies conducted with these nucleophiles have shown the reactivity trend to depend upon the basicity of the nitrogen which coordinates to the Pt(II) centre during substitution reactions [27,46,49]. Since azoles are potential ambidentate ligands, assurance as to which binding site is more preferred for coordination is essential. For this reason, computational DFT studies were performed on the nucleophiles in the gaseous phase and the data obtained are represented in Table 5.

From the NBO charges, it is clear that for MIm and DIm nucleophiles, the pyridinic-N (N2 in Table 5) has a more negative charge than the pyrrolic-N (N1 in Table 5). This is due to the ability of the pyrrolic-N to donate electrons towards the electronic ring system, making the pyridinic-N more negative and thus more reactive towards electrophilic centres [49,50]. For **Trz**, the N3-pyridinic position is more preferred for binding to electrophiles than the N1 and N2 position. This is because the NBO charge of N3 (−0.490) is more negative than the NBO charges of N1 (−0.431) and N2 (−0.272). Furthermore, the crystal structures of azole coor-

dinated Pt(II) complexes have been reported and NBO charges are in line with the binding sites predicted by the computational data [49,51,52].

In this study, the reactivity of the azole nucleophiles with no substituents, **Pyz**, **Im** and **Trz**, were found to follow the trend **Im** > **Trz** > **Pyz**. This trend is in line with the basicity of the nucleophiles, whose pK_a values are **Im** = 7.00, **Pyz** = 2.52 and **Trz** = 2.19 as summarised in Table 5 [53,54].

For the studied complexes and nucleophiles, the negative entropy values, $\Delta S^{\neq}$ for the substitution reactions support an associative mechanism that is typical of Pt(II) d^8 square planar complexes [7,24].

6. Conclusion

The results of this study reveal that the lability of the aqua ligand of **Ptdpa** and **Ptdps** is strongly influenced by the strength of the σ-donation character of the atom *trans* to the leaving group as previously reported [18,45,55,56,27,57–59]. The S-atom in **Ptdps** is both a strong σ-donor and a π-acceptor. It uses its unoccupied *d*-orbitals for σ/π-back bonding, allowing electron density from the metal to be transferred to these *d*-orbitals, leading to a more electrophilic Pt-centre, stabilizes the transition state more and leads to a higher reactivity. Therefore, the higher reactivity of **Ptdps** compared to **Ptdpa** is due to a strong *trans*-effect in combination with π-back bonding as supported by the DFT calculations. The effect on reactivity is very similar to what has been observed for the chloro complex of the **Pt(NCN)**Cl [45].

A general conclusion can be made looking at the current study and what is currently in the literature including the chloro complexes of the coordinated NCN platinum complexes [45]. That is, that the final product of the substitution reactions involving the azole nucleophiles are more stable compared to those of the S-donor nucleophiles such as thiourea which show dechelation of the ligand [18,55,56] with time. This is mostly due to the weakness of the azole as nucleophiles compared to the thioureas. It can also be stated that the Pt-$N_{pyridyl}$, the Pt-S_{trans} and the Pt-C_{trans} bonds in the complex chelate are stronger compared to that of the N-atom from azoles. The stability of the azole complexes is an indication of a reduced toxicity of the complexes when they interact with plasma proteins before they react with nucleic acids, a problem which is encountered by many Pt anticancer drugs.

The reactivity of the nucleophiles investigated was found to be influenced by both steric factors (**DIm**, **MIm** and **Im**) and electronic factors (**Im**, **Pyz** and **Trz**). The reactivity-nucleophile basicity LFER of all the heterocyclic nucleophiles investigated showed that **Ptdps** was more sensitive to changes in the nature of the nucleophiles than **Ptdpa**.

Acknowledgements

The authors thank the University of KwaZulu-Natal and the National Research Foundation (NRF, South Africa) for financial support and a bursary to S. V. N.

Appendix A. Supplementary data

Supplementary data associated with this article can be found, in the online version, at http://dx.doi.org/10.1016/j.ica.2017.05.054.

References

[1] B. Rosenberg, L. Van Champ, J.E. Trosko, V.H. Mansour, Nature 222 (1969) 385.
[2] B. Rosenberg, Cancer 55 (1985) 2303.
[3] B. Lippert, Cisplatin: Chemistry and Biochemistry of a Leading Anticancer Drug, Wiley-VCH, New York, 1999. 1–100, 184–190.
[4] E. Wong, C.M. Giandomenico, Chem. Rev. 99 (1999) 2451.
[5] C.D. Hubbard, R. van Eldik, J. Coord. Chem. 60 (1) (2007) 1–51.
[6] M.L. Tobe, J. Burgess, Inorganic Reaction Mechanisms, Longman, Harlow, Essex, England; New York, 1999.
[7] F. Basolo, J. Chat, H.B. Gray, R.G. Pearson, B.L. Shaw, J. Chem. Soc. (1961) 2207.
[8] M. Schmulling, A.D. Ryabov, R. van Eldik, J. Chem. Soc., Chem. Commun. (1992) 1609.
[9] D. Jaganyi, F. Tiba, Transition Met. Chem. 28 (2003) 803.
[10] D. Jaganyi, F. Tiba, O.Q. Munro, B. Petrović, Ž.D. Bugarčić, Dalton Trans. (2006) 2943.
[11] Ž.D. Bugarčić, G. Liehr, R. van Eldik, J. Chem. Soc., Dalton Trans. (2001) 2825.
[12] Ž.D. Bugarčić, G. Liehr, R. van Eldik, J. Chem. Soc., Dalton Trans. (2002) 951.
[13] B. Pitteri, E.I.J. Breet, R. van Eldik, Inorg. Chim. Acta 301 (1983) 76.
[14] B. Pitteri, G. Marangoni, L. Cattalini, T. Bobbo, J. Chem. Soc., Dalton Trans. (1995) 3853.
[15] G. Annibale, M. Brandolisio, Ž.D. Bugarčić, L. Cattalini, Transition Met. Chem. 23 (1998) 715.
[16] A. Hofmann, L. Dahlenburg, R. van Eldik, Inorg. Chem. 42 (2003) 6528.
[17] B. Petrović, Ž.D. Burgarčić, A. Dees, I. Ivanović-Burmazović, F.W. Heinemann, R. Puchta, S.N. Steinmann, C. Corminboeuf, R. van Eldik, Inorg. Chem. 51 (2012) 1516.
[18] A. Mambanda, D. Jaganyi, Dalton Trans. 40 (2011) 79.
[19] D. Jaganyi, D. Reddy, J.A. Gertenbach, A. Hofmann, R. van Eldik, Dalton Trans. (2004) 299.
[20] S. Hochreuther, S.T. Nandibewoor, R. Puchta, R. van Eldik, Dalton Trans. 41 (2012) 512.
[21] G. Bogdanović, V. Kojić, T. Srdić, D. Jakimov, M. Djuran, Ž.D. Bugarčić, M. Baltić, V.V. Baldić, Metal Based Drugs 9 (2002) 33.
[22] B. Pitteri, M. Bortoluzzi, G. Marangoni, Transition Met. Chem. 30 (2005) 1008.
[23] L.R. Kelland, N.P. Farrell, Platinum-Based Drugs in Cancer Therapy, Humana Press, 2000, pp. 321–337.
[24] J.D. Atwood, Inorganic and Organometallic Reaction Mechanisms, second ed., Wiley-VCH, New York Inc., Canada, 1997.
[25] R.G. Wilkinson, Kinetics and Mechanism of Reactions at Transition Metal Complexes, second ed., VCH, Weinheim, 1991. 199–201, 232–242.
[26] P. Banerjee, Coord. Chem. Rev. 190–192 (1999) 19–28.
[27] D. Reddy, K.J. Akerman, M.P. Akerman, D. Jaganyi, Transition Met. Chem. 36 (2011) 593.
[28] R.J. Sundberg, R.B. Martin, Chem. Rev. 74 (1974) 471.
[29] C.A. Hitchcock, Biochem. Soc. Trans. 19 (1991) 782.
[30] M.A. Jalil, S. Fujinami, H. Senda, H. Nishikawa, J. Chem. Soc., Dalton Trans. (1999) 1655.
[31] R. Contreras, A. Flores-Parra, E. Mijangos, F. Telles, H. Lopez-Sandoval, N. Barba-Behenens, Coord. Chem. Rev. 253 (2009) 1979.
[32] N.-D. Sung, K.-Y. Choi, H.-H. Lee, K.-C. Lee, M.-J. Kim, Transition Met. Chem. 30 (2005) 273.
[33] A. Hofmann, D. Jaganyi, O.Q. Munro, G. Liehr, R. van Eldik, Inorg. Chem. 42 (2003) 1688.
[34] B. Pitteri, G. Marangoni, L. Cattalini, Polyhedron 14 (1995) 2331.
[35] Origin7.5TM SRO, v7.5714 (B5714), Origin Lab Corporation, Northampton, One, Northampton, MA, 01060, USA, 2003.
[36] Bruker APEX2, SAINT and SADABS. Bruker AXS Inc., Madison, Wisconsin, USA, (2010).
[37] G.M. Sheldick, A short history of SHELX, Acta Crystallogr., Sect. A 64 (2008) 112.
[38] O.V. Dolomanov, L.J. Bourhis, R.J. Gildea, J.A.K. Howard, H. Puschmann, J. Appl. Cryst. 42 (2009) 229.
[39] M.J. Frisch, G.W. Trucks, H.B. Schlegel, G.E. Scuseria, M.A. Robb, J.R. Cheeseman, G. Scalmani, V. Barone, B. Mennucci, G.A. Petersson, H. Nakatsuji, M. Caricato, X. Li, H.P. Hratchian, A.F. Izmaylov, J. Bloino, G. Zheng, J.L. Sonnenberg, M. Hada, M. Ehara, K. Toyota, R. Fukuda, J. Hasegawa, M. Ishida, T. Nakajima, Y. Honda, O. Kitao, H. Nakai, T. Vreven, J.A. Montgomery Jr., J.E. Peralta, F. Ogliaro, M. Bearpark, J.J. Heyd, E. Brothers, K. N. Kudin, V.N. Staroverov, R. Kobayashi, J. Normand, K. Raghavachari, A. Rendell, J.C. Burant, S.S. Iyengar, J. Tomasi, M. Cossi, N. Rega, J.M. Millam, M. Klene, J.E. Knox, J.B. Cross, V. Bakken, C. Adamo, J. Jaramillo, R. Gomperts, R. E. Stratmann, O. Yazyev, A.J. Austin, R. Cammi, C. Pomelli, J.W. Ochterski, R.L. Martin, K. Morokuma, V.G. Zakrzewski, G.A. Voth, P. Salvador, J.J. Dannenberg, S. Dapprich, A.D. Daniels, O. Farkas, J.B. Foresman, J.V. Ortiz, J. Cioslowski, and D.J. Fox, Gaussian 09, Revision C.1, Gaussian Inc., Wallingford, CT, 2010.
[40] J.C. Bailar, H.J. Emeléus, R. Nyholm, A.F. Trotman-Dickenson, Comprehensive Inorganic Chemistry, Pergamon press, Oxford, New York, 1973, pp. 795–931.
[41] F.A. Cotton, G. Wilkinson, Advanced Inorganic Chemistry, 5th edition., Wiley-Interscience, New York, 1988, pp. 491–543.
[42] M. Schmulling, D.M. Grove, G. van Koten, R. van Eldik, N. Veldman, A.L. Spek, Organometallics 15 (1996) 1384.
[43] U. Belluco, L. Cattalini, F. Basolo, R.G. Pearson, A. Turco, J. Am. Chem. Soc. 87 (1965) 241.
[44] L. Dadci, H. Elias, U. Frey, A. Hörnig, U. Koelle, A.E. Merbach, H. Paulus, J.S. Schneider, Inorg. Chem. 34 (1995) 306.
[45] T.R. Papo, D. Jaganyi, Transition Met. Chem. 40 (2015) 53.
[46] B. Pitteri, M. Bortoluzzi, Polyhedron 25 (2006) 2698.
[47] B. Pitteri, G. Marangoni, L. Cattalini, F. Visentin, V. Bertolasi, P. Gilli, Polyhedron 20 (2001) 869.
[48] B. Pitteri, M. Bortoluzzi, Eur. J. Inorg. Chem. 28 (2007) 4456.

[49] A. Shaira, D. Reddy, D. Jaganyi, Dalton Trans. 42 (2013) 8426.
[50] A.R. Katritzky, A.F. Pozharski, Handbook of Heterocyclic Chemistry, Second ed., Pergamon/Elsevier, London, 2000. 177, 377.
[51] M. Akerman, K. Akerman, D. Jaganyi, D. Reddy, Acta Cryst. E67 (2011) m1075.
[52] M. Akerman, K. Akerman, D. Jaganyi, D. Reddy, Acta Cryst. C67 (2010) m290.
[53] A.R. Katritzky, C.W. Rees, Comprehensive Heterocyclic Chemistry, vol 5, Pergamon Press, Oxford, 1984. p. 35–50, 169–225.
[54] T. Eicher, S. Hauptmann, The Chemistry of Heterocycles, Wiley-VCH Verlas GmbH & Co. KGaA, Weinheim, 2003. 165–173, 179–184, 208–212.
[55] A. Mambanda, D. Jaganyi, Dalton Trans. 41 (2012) 908.
[56] A. Mambanda, D. Jaganyi, S. Hochreuther, R. van Eldik, Dalton Trans. 39 (2010) 3595.
[57] G. Enos, A. Mambanda, D. Jaganyi, J. Coord. Chem. 66 (2013) 4280.
[58] M. Chipangura, A. Mambanda, D. Jaganyi, J. Coord. Chem. 67 (2014) 2048.
[59] Ž.D. Burgarčić, A.T. Nandibewoor, M.S.A. Hamza, F. Heinemann, R. van Eldik, Dalton Trans. 24 (2006) 2984.